Journal of the Korean Ceramic Society
Vol. 40, No. 4, pp. 354~359, 2003.

Microwave Dielectric Characteristics of Aluminum Magnesium Tantalate Based High Q Ceramics

Ji-Won Choi,† Hwack-Joo Lee,* Seok-Jin Yoon, and Hyun-Jai Kim

Thin Film Materials Research Center, Korea Institute of Science and Technology, Seoul 130-650, Korea
**New Materials Evaluation Center, Korea Research Institute of Standard and Science, Taejon 305-600, Korea*
(Received March 19, 2003; Accepted March 29, 2003)

ABSTRACTS

The microwave dielectric characteristics of $(1-x)(Al_{1/2}Ta_{1/2})O_2$-$x(Mg_{1/3}Ta_{2/3})O_2$ $(0 \le x \le 1.0)$ ceramics were investigated by crystal structure, variations of ionic polarizability, and microstructures. As x increased, $(1-x)(Al_{1/2}Ta_{1/2})O_2$-$x(Mg_{1/3}Ta_{2/3})O_2$ transformed to tetragonal structure. Because the ionic radius of $[Mg_{1/3}Ta_{2/3}]^{4+}$ was slightly bigger than one of $[Al_{1/2}Ta_{1/2}]^{4+}$, the cell parameters increased with increase of $(Mg_{1/3}Ta_{2/3})O_2$ concentration and coincided with prediction of the molecular additivity rule. As x increased, the compositions revealed ordered phase and were of single phase above 60 mol%. The increase of the ordered phase and grain size enhanced the Q and when ordering was completed at x over 0.6, the grain size was major factor for the increase in the Q. Though the grain size increased, however, the porosity deteriorated the Q. Therefore, the Q depended on the order/disorder, the porosity, and the grain size in regular order.

Key words : Microwave dielectric materials, Dielectric constant, Quality factor, Ionic polarizability, Ordering

1. Introduction

Recently, the use of high frequency dielectric ceramics for applications such as resonators, band pass (stop) filters, duplexers, antennas has increased in the practical use of mobile communications such as cellular (800 MHz), PCS (1.9 GHz), IMT2000 (2 GHz), and UMTS (3–4 GHz).[1,2] Therefore, materials for microwave application have to exhibit three dielectric characteristics,[3-8] namely relatively low dielectric constant (ε_r), high quality factor (Q), and stable ($\approx$0 ppm/°C) temperature coefficient of the resonant frequency (τ_f). Among these requirements, the dielectric constant and the temperature coefficient of resonant frequency depend on composition and the dielectric loss depends on phonon anharmonic interaction, porosity, grain size, impurity, defects, etc. Therefore, the investigation of methods to predict for these three characteristics is necessary.

The purpose of the present work is to predict and compare with the experimental dielectric constant for $(1-x)(Al_{1/2}Ta_{1/2})O_2$-$x(Mg_{1/3}Ta_{2/3})O_2$ solid solutions using dielectric mixing rule from Vegards law and the molecular additivity rule based on ionic polarizability and crystallographic data. The dielectric constants (ε_r) of aluminum tantalate and magnesium tantalate which are B-site of complex perovskites were 9.3 and 27.4, respectively. The other purpose of the present work is to establish the extrinsic dielectric loss mechanism for $(1-x)(Al_{1/2}Ta_{1/2})O_2$-$x(Mg_{1/3}Ta_{2/3})O_2$ ceramics based upon microstructures obtained by Scanning Electron Microscopy (SEM) and Transmission Electron Microscopy (TEM). The effects of order/disorder, grain size, and porosity on the Q factor are discussed.

†Corresponding author : Ji-Won Choi
E-mail : jwchoi@kist.re.kr
Tel : +82-2-958-5556 Fax : +82-2-958-6720

2. Experimental Procedures

$(1-x)(Al_{1/2}Ta_{1/2})O_2$-$x(Mg_{1/3}Ta_{2/3})O_2$ $(0 \le x \le 1.0)$ powder compositions were synthesized using the conventional solid-state reaction method. The starting materials were Al_2O_3 (Aldrich, 99.7%), Ta_2O_5 (Aldrich, 99%), and MgO (Aldrich, 98%). Stoichiometric compositions were mixed for 24 h with stabilized ZrO_2 media and distilled water, then dried and calcined. The calcined powders were re-milled and pressed into discs of 12 mm in diameter and 6 mm in thickness under a pressure of 150 MPa. The pellets were sintered at 1450°C for 3 h in air. The sintered specimens were ground and polished to precise dimensions to achieve the ratio of thickness to diameter of 0.4–0.5.

X-Ray Diffractometry (XRD, Cu Kα radiation, Model Rint/Dmax 2500, Rigaku, Japan) was conducted on powders obtained by crushing the sintered specimens for phase identification and lattice parameter measurements. The bulk densities of the sintered pellets were determined by the Archimedes method. The microstructures of the sintered specimens were investigated using SEM (Model S-4200, Hitachi, Japan) and TEM (Model H9000-NAR, Hitachi, Kastsuda, Ibaraki, Japan). The polished surfaces of the ceramics were investigated by SEM after thermal etching at 1380°C for 20 min in air. The TEM specimens were pre-

pared by ultrasonic cutting 3 mm diameter disks and mechanical polishing them to a thickness of ~100 μm. The central parts of the disks were further reduced to ~10 μm by mechanical dimpling followed by final polishing. The final perforation of the specimen was conducted by precision argon-ion milling (Model 691 Gatan, San Francisco, CA) with an acceleration voltage of 3 KeV. These specimens were examined using a side-entry-type high resolution TEM operated at 300 KV with a point resolution of 0.18 nm. The Selected Area Diffraction (SAD) and bright field TEM (BF-TEM) images could be obtained. The dielectric properties were measured at 6–11 GHz using the parallel-plate (Hakki and Coleman) method interfaced with a network analyzer (HP-8720C, Hewlett Packard, USA).[9]

3. Results and Discussion

Fig. 1 shows x-ray diffraction patterns for (1-x)$(Al_{1/2}Ta_{1/2})O_2$-x$(Mg_{1/3}Ta_{2/3})O_2$ ceramics sintered at 1450°C for 3 h. The diffraction peaks can be indexed based on orthorhombic $(Al_{1/2}Ta_{1/2})O_2$ and tetragonal $(Mg_{1/3}Ta_{2/3})O_2$ with four formula units per unit cell. As x increased, (1-x)$(Al_{1/2}Ta_{1/2})O_2$-x$(Mg_{1/3}Ta_{2/3})O_2$ transformed into tetragonal structure. The tetragonal single phase was obtained in the range of 0.6=x=1.0. Some of the crystallographic data for (1-x)$(Al_{1/2}Ta_{1/2})O_2$-x$(Mg_{1/3}Ta_{2/3})O_2$ are listed in Table 1 and the unit cell parameters are derived from a computerized least-squares refinement technique.[10] The unit cell parameters generally increased with an increase of $(Mg_{1/3}Ta_{2/3})O_2$ concentration because of the difference of average ionic radii of $[Al^{+3}+Ta^{+5}]/2$ (0.059 nm) and $[Mg^{+2}+2Ta^{+5}]/3$ (0.067 nm).[11] This was confirmed from the shift of 2 peaks of the X-ray diffraction patterns to smaller values with increasing $(Mg_{1/3}Ta_{2/3})O_2$ concentration.

Fig. 2 shows the measured and the calculated dielectric constants as a function of x for (1-x)$(Al_{1/2}Ta_{1/2})O_2$-x$(Mg_{1/3}Ta_{2/3})O_2$ ceramics sintered at 1450°C for 3 h. The dielectric constant may be calculated from Vegards law[12] using equation (1):

$$k = (1-x)k(AT) + xk(MT) \quad (1)$$

where $k(AT)$ and $k(MT)$ are the dielectric constants of $(Al_{1/2}Ta_{1/2})O_2$ and $(Mg_{1/3}Ta_{2/3})O_2$.

The dielectric constant may also be calculated from the molecular additivity rule[13] using ionic polarizability and

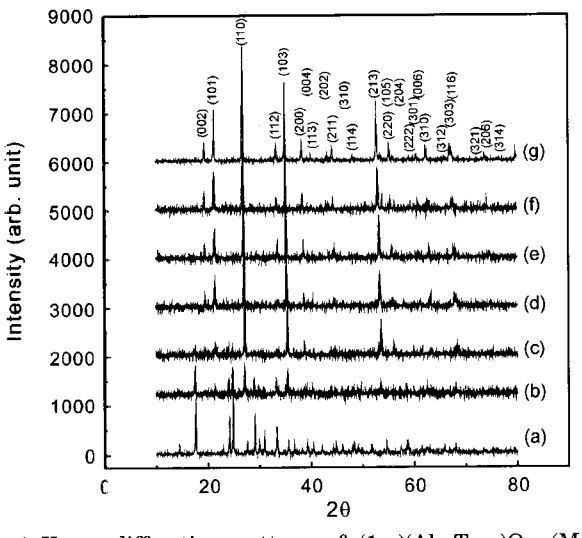

Fig. 1. X-ray diffraction pattern of (1-x)$(Al_{1/2}Ta_{1/2})O_2$-x$(Mg_{1/3}Ta_{2/3})O_2$ ceramics sintered at 1450°C for 3 h : (a) x=0, (b) x=0.2, (c) x=0.4, (d) x=0.6, (e) x=0.65, (f) x=0.8, and (g) x=1.0.

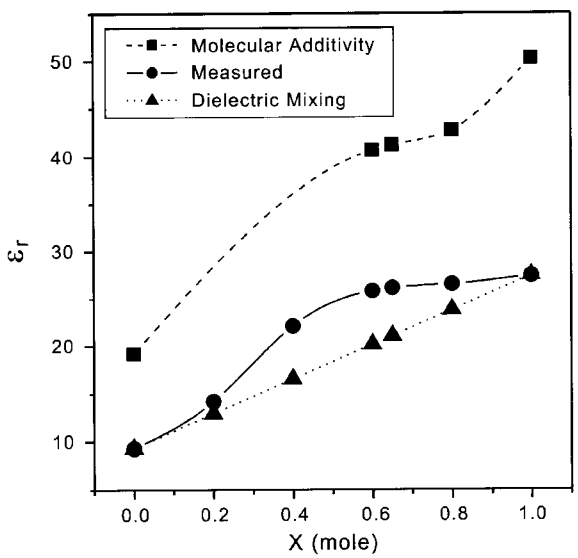

Fig. 2. The measured and the calculated dielectric constant as a function of x for (1-x)$(Al_{1/2}Ta_{1/2})O_2$-x$(Mg_{1/3}Ta_{2/3})O_2$ ceramics sintered at 1450°C for 3 h.

Table 1. Crystallographic Data for (1-x)$(Al_{1/2}Ta_{1/2})O_2$-x$(Mg_{1/3}Ta_{2/3})O_2$ Ceramics Sintered at 1450°C for 3 h

x	Orthorhombic			Tetragonal		Vol per unit cel ($\times 10^{-3}$ nm^3)	X-ray density (g/cm^3)
	a ($\times 10^{-1}$ nm)	b ($\times 10^{-1}$ nm)	c ($\times 10^{-1}$ nm)	a ($\times 10^{-1}$ nm)	c ($\times 10^{-1}$ nm)		
0	6.1340	7.3620	8.7912	X	X	397.00	6.8222
0.2	6.1410	7.3981	8.8506	4.6406	9.0593	X	X
0.4	6.1364	7.4090	8.8742	4.6354	9.0444	X	X
0.6	X	X	X	4.6543	9.0851	196.80	7.6332
0.65	X	X	X	4.6619	9.0986	197.74	7.6595
0.8	X	X	X	4.6843	9.1429	200.61	7.7342
1.0	X	X	X	4.7602	9.1710	203.02	7.8854

Table 2. Calculated Dielectric Constants for (1-x)$(Al_{1/2}Ta_{1/2})O_2$-x$(Mg_{1/3}Ta_{2/3})O_2$ Solid Solutions Sintered at 1450°C for 3 h Based on Dielectric Polarizability Data

x	α_D	$V_{unit\text{-}cell}$	Z	V_m	K_{cal}
0	13.56	397.00	6	66.17	19.19
0.6	21.84	196.80	2	98.40	40.68
0.65	21.97	197.74	2	98.87	41.22
0.8	22.34	200.60	2	100.30	42.76
1.0	22.84	203.02	2	101.50	50.25

lattice parameter data as follows (Table II):

$$\alpha_D(M_2M'X_4) = 2\alpha_D(MX) + \alpha_D(M'X_2)$$
$$= 2\alpha(M^{2+}) + \alpha(M'^{4+}) + 4\alpha(X^{2-}) \quad (2)$$

where α_D and α are dielectric and ionic polarizability.

$$k' = \frac{(3V_m + 8\pi\alpha_D^T)}{(3V_m - 4\pi\alpha_D^T)} \quad (3)$$

where k' is the dielectric constant and V_m is molar volume, and α_D is total ionic polarizability.

The measured dielectric constants of $(Al_{1/2}Ta_{1/2})O_2$ and $(Mg_{1/3}Ta_{2/3})O_2$ are 9.3 and 27.4, respectively. As the $(Mg_{1/3}Ta_{2/3})O_2$ concentration having high dielectric constant increased from 0 to 60 mole%, the measured dielectric constant increased from 9.3 to 25.8. As the $(Mg_{1/3}Ta_{2/3})O_2$ concentration increased from 60 to 100 mole%, however, the measured dielectric constant increased only slightly from 25.8 to 27.4. The calculated dielectric constant, using molecular additivity rule, increased from 19.2 to 50.3 as the $(Mg_{1/3}Ta_{2/3})O_2$ concentration increased from 0 to 100 mole%, these values compare well with the experimental results. It was found that the measured values were lower than the calculated values due to the electronic structure of tantalum. Tantalum ion has vacant 5d-orbital and prefers to ionic bonding. The niobium ion prefers covalent bonding. The ionic radius of tantalum and niobium is nearly same as 0.064 nm. It is reported that the Nb-O bond length in case of MNb_2O_6 is 2.015 to 2.021. However, the Ta-O bond length in case of MTa_2O_6 is 1.989 to 2.009.[14] Therefore, it can be thought that tantalum ion was subjected compressive stress which decreased the actual dielectric constant. This result shows that it is possible to predict the behavior of dielectric constant using molecular additivity rule and crystallographic data if we know the dielectric constant of the end members.

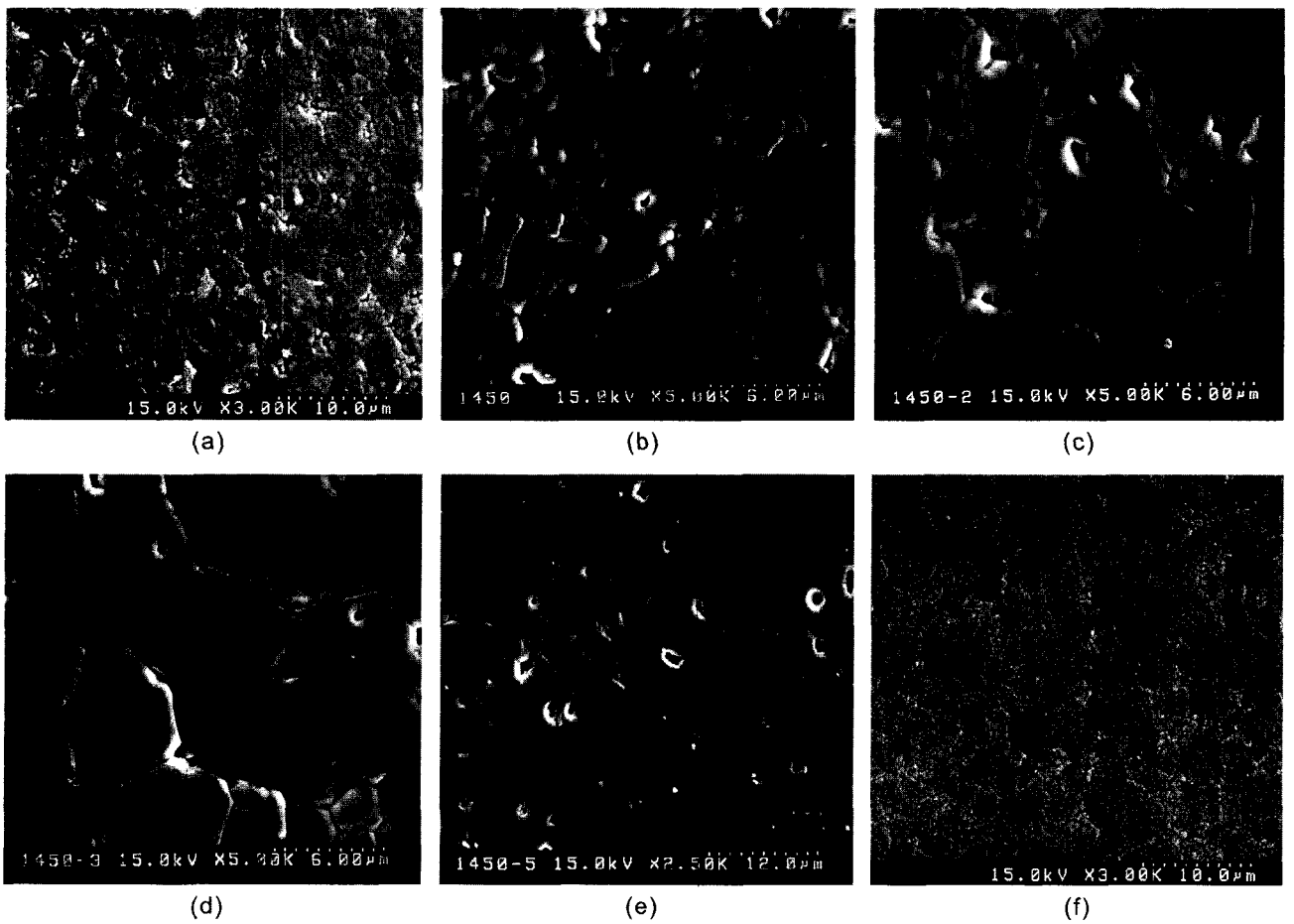

Fig. 3. SEM photographs of (1-x)$(Al_{1/2}Ta_{1/2})O_2$-x$(Mg_{1/3}Ta_{2/3})O_2$ ceramics sintered at 1450°C for 3 h: (a) x=0, (b) x=0.2, (c) x=0.4, (d) x=0.6, (e) x=0.8, and (f) x=1.0.

The trends for the calculated dielectric constant, using Vegards law closely, compare well with the measured ones.

Fig. 3 shows SEM photographs of $(1-x)(Al_{1/2}Ta_{1/2})O_2$-$x(Mg_{1/3}Ta_{2/3})O_2$ ceramics sintered at 1450°C for 3 h. It is necessary to note that the SEM photographs have different magnifications for convenience. $(Al_{1/2}Ta_{1/2})O_2$ (Fig. 3(a)) has a small grain size. As the $(Mg_{1/3}Ta_{2/3})O_2$ concentration increases from 20 to 65 mole%, the grain size increases from 2 to 12 μm and porosity decreases. When $(Mg_{1/3}Ta_{2/3})O_2$ concentration is 80 mole%, however, the grain size is significantly large (15 μm) and the pore size inside the grains is also large. The decrease of apparent density at $(Mg_{1/3}Ta_{2/3})O_2$ concentration of 80 mole% stems from these increase of porosity as shown in Fig. 4. It is an interesting result that $(Mg_{1/3}Ta_{2/3})O_2$ (Fig. 3(f)) has small grain size.

Fig. 5 shows the SAED patterns for $(1-x)(Al_{1/2}Ta_{1/2})O_2$-$x(Mg_{1/3}Ta_{2/3})O_2$ ceramics sintered at 1450°C for 3 h. $(Al_{1/2}Ta_{1/2})O_2$ (Fig. 5(a)) does not show any ordered phase. $(Mg_{1/3}Ta_{2/3})O_2$ (Fig. 5(e)) shows 1:2 ordered tri-rutile structure. As $(Mg_{1/3}Ta_{2/3})O_2$ concentration increased from 20 to 40 mole%, the ordered phase starts to appear and is mixed with disordered one. In the case of $(Mg_{1/3}Ta_{2/3})O_2$ concentration over 60 mole%, $(1-x)(Al_{1/2}Ta_{1/2})O_2$-$x(Mg_{1/3}Ta_{2/3})O_2$ ceramics shows fully 1:2 ordered phase.

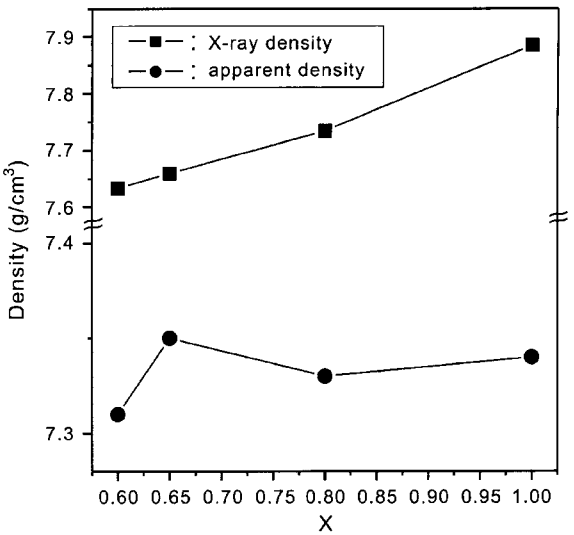

Fig. 4. Densities for $(1-x)(Al_{1/2}Ta_{1/2})O_2$-$x(Mg_{1/3}Ta_{2/3})O_2$ ceramics sintered at 1450°C for 3 h.

Fig. 6 shows the BF-TEM images for $(1-x)(Al_{1/2}Ta_{1/2})O_2$-$x(Mg_{1/3}Ta_{2/3})O_2$ ceramics sintered at 1450°C for 3 h. These images agree with SAED patterns shown in Fig. 4. $(Al_{1/2}Ta_{1/2})O_2$ (Fig. 6(a)) does not show any anti-phase boundaries

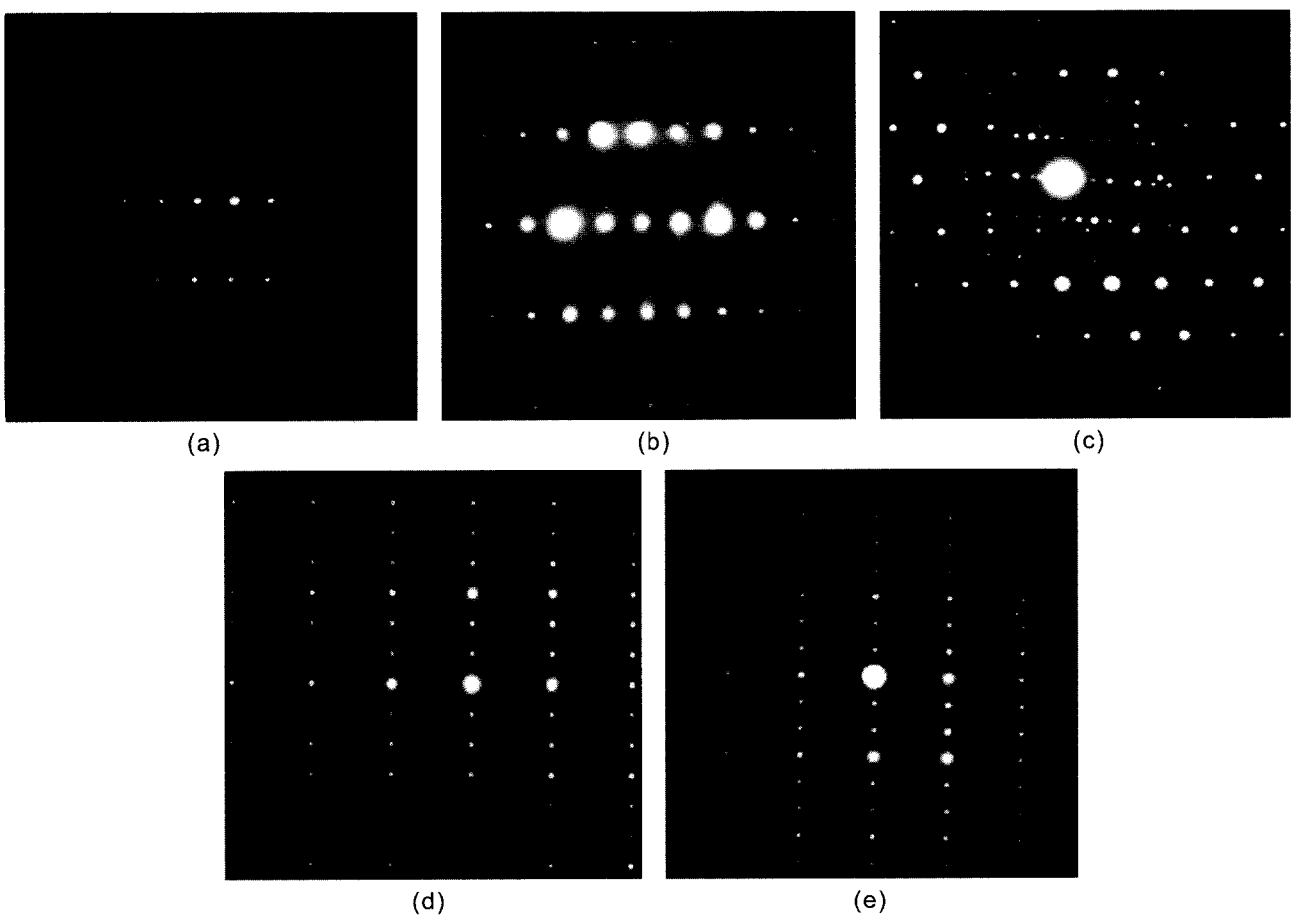

Fig. 5. SAED patterns of $(1-x)(Al_{1/2}Ta_{1/2})O_2$-$x(Mg_{1/3}Ta_{2/3})O_2$ ceramics sintered at 1450°C for 3 h: (a) x=0 with [001] zone axes, (b) x=0.2 with [001] zone axes, (c) x=0.4, (d) x=0.6 with [1$\bar{1}$0] zone axes, and (e) x=1.0 with [1$\bar{1}$0] zone axes.

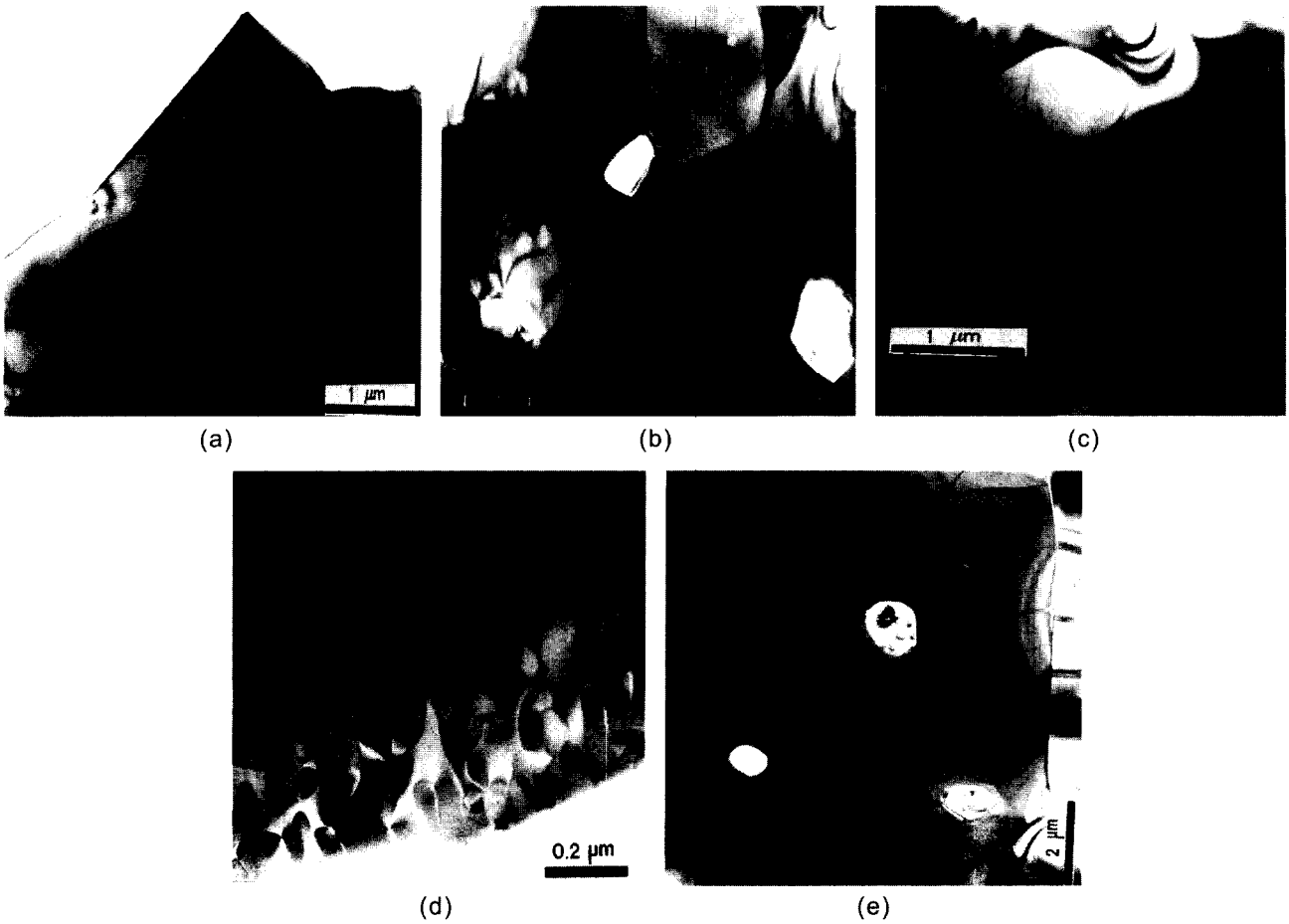

Fig. 6. BF-TEM images of (1-x)$(Al_{1/2}Ta_{1/2})O_2$-x$(Mg_{1/3}Ta_{2/3})O_2$ ceramics sintered at 1450°C for 3 h: (a) x=0, (b) x=0.2, (c) x=0.4, (d) x=0.6, and (e) x=1.0.

(APBs).[15] This means $(Al_{1/2}Ta_{1/2})O_2$ is not an ordered phase. $(Mg_{1/3}Ta_{2/3})O_2$ (Fig. 6(e)) shows APBs. As the $(Mg_{1/3}Ta_{2/3})O_2$ concentration increases from 20 to 40 mole%, the APBs start to appear and when $(Mg_{1/3}Ta_{2/3})O_2$ concentration is 60 mole%, (1-x)$(Al_{1/2}Ta_{1/2})O_2$-x$(Mg_{1/3}Ta_{2/3})O_2$ ceramics show many APBs.

Fig. 7 shows the $Q{\cdot}f_0$ variation for (1-x)$(Al_{1/2}Ta_{1/2})O_2$-x$(Mg_{1/3}Ta_{2/3})O_2$ ceramics sintered at 1450°C for 3 h. As $(Mg_{1/3}Ta_{2/3})O_2$ concentration increased from 0 to 65 mole%, the $Q{\cdot}f_0$ linearly increases from 30900 to 112500 GHz, and slightly decreases to 103200 GHz at 80 mole% and then increases again to 117200 GHz at 100 mole%. The variation of $Q{\cdot}f_0$ can be explained by microstructures. As shown in Figs. 5(a), (e) and 6(a), (e), $(Al_{1/2}Ta_{1/2})O_2$ is not ordered and $(Mg_{1/3}Ta_{2/3})O_2$ has an 1:2 ordered trirutile structure. These compositions have small grain size and porosity in comparison with $(Al_{1/2}Ta_{1/2})O_2$-$(Mg_{1/3}Ta_{2/3})O_2$ compounds shown in SEM photographs (Fig. 3(b)-(e)). The large difference of $Q{\cdot}f_0$ between $(Al_{1/2}Ta_{1/2})O_2$ (30900 GHz) and $(Mg_{1/3}Ta_{2/3})O_2$ (117200 GHz) is not generated from grain size or porosity but is due to cation ordering. On the other hand, Fig. 7 can be divided into two regions which are 0 to 60 mole% and 60 to 100 mole%. As $(Mg_{1/3}Ta_{2/3})O_2$ concentration increases from 0 to 60 mole%,

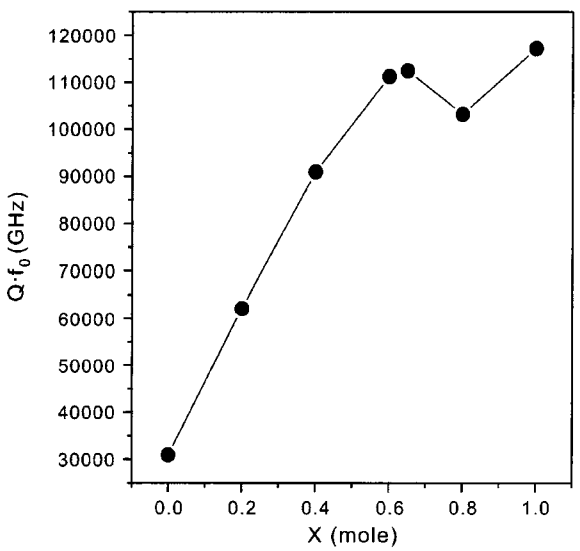

Fig. 7. $Q{\cdot}f_0$ value of (1-x)$(Al_{1/2}Ta_{1/2})O_2$-x$(Mg_{1/3}Ta_{2/3})O_2$ ceramics sintered at 1450°C for 3 h.

the $Q{\cdot}f_0$ linearly increases, and the ordering started from 20 mole% and completed at 60 mole% shown in Figs. 5(b)-(d)

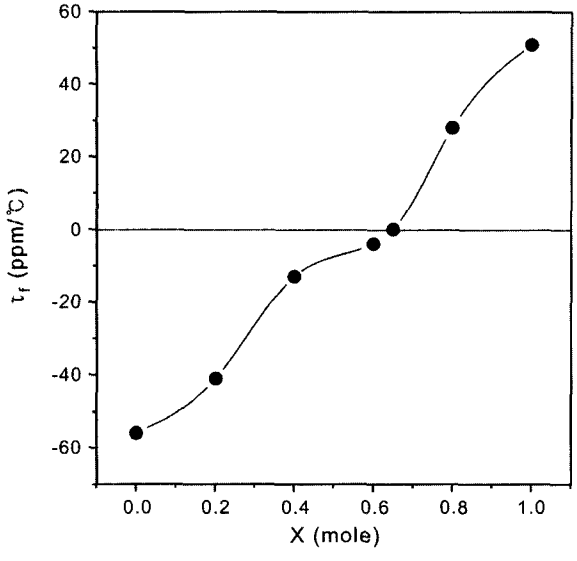

Fig. 8. τ_f of $(1\text{-}x)(Al_{1/2}Ta_{1/2})O_2\text{-}x(Mg_{1/3}Ta_{2/3})O_2$ ceramics sintered at 1450°C for 3 h.

and 6(b)-(d). Of course, the grain size also rapidly increases in the region. As $(Mg_{1/3}Ta_{2/3})O_2$ concentration increases from 60 to 100 mole%, the $Q{\cdot}f_0$ varies, with both increase and decrease but the $Q{\cdot}f_0$ variation is small. The ordering state is nearly the same as shown in Fig. 5(d)-(e) but the grain size also increases rapidly in the region. The decrease of $Q{\cdot}f_0$ at 80 mole% is due to the increase of porosity in grains. From these results, the variation of $Q{\cdot}f_0$ due to ordering is dominant, however the variation of $Q{\cdot}f_0$ due to grain size is not so large as ordering and when the porosity in grain increases, the $Q{\cdot}f_0$ decreases though the grain size increases. Therefore, the main factor which affects the $Q{\cdot}f_0$ is cation order/disorder and the grain size is secondly important factor and $Q{\cdot}f_0$ depends on not only the grain size but also the porosity in grains.

Fig. 8 shows τ_f of the $(1\text{-}x)(Al_{1/2}Ta_{1/2})O_2\text{-}x(Mg_{1/3}Ta_{2/3})O_2$ ceramics sintered at 1450°C for 3 h. The τ_f value increased from 56 to 51 ppm/°C with an increase of $(Mg_{1/3}Ta_{2/3})O_2$ having positive τ_f value. A τ_f value of 0 ppm/°C was realized for $0.35(Al_{1/2}Ta_{1/2})O_2\text{-}0.65(Mg_{1/3}Ta_{2/3})O_2$ (x=0.65). This composition has ε_r and $Q{\cdot}f_0$ value of 26.1 and 112470 GHz respectively.

4. Conclusions

The dielectric characteristics of $(1\text{-}x)(Al_{1/2}Ta_{1/2})O_2\text{-}x(Mg_{1/3}Ta_{2/3})O_2$ ceramics were investigated by crystal structure, variations of ionic polarizability and microstructures. The behavior of calculated dielectric constant using molecular additivity rule coincided with the measured result. It is possible to predict the behavior of dielectric constant using molecular additivity rule and crystallographic data if we know the dielectric constant of the end members. The trends for the calculated dielectric constant, using Vegards law closely, compare well with the measured ones. The extrinsic loss of microwave dielectrics depended on cation ordering, grain size, and porosity. The variations of $Q{\cdot}f_0$ due to ordering is very large, however those of $Q{\cdot}f_0$ due to grain size is not large when the porosity in grains increase, the $Q{\cdot}f_0$ decreases though the grain size increases. Therefore, the main factor increasing the $Q{\cdot}f_0$ is cations order/disorder and the grain size is secondly important factor and $Q{\cdot}f_0$ depends on not only the grain size but also the porosity in grains. A τ_f value of 0 ppm/°C was realized for $0.35(Al_{1/2}Ta_{1/2})O_2\text{-}0.65(Mg_{1/3}Ta_{2/3})O_2$ (x=0.65). This composition has ε_r and $Q{\cdot}f_0$ value of 26.1 and 112470 GHz respectively.

REFERENCES

1. H. Hughes, D. M. Iddles, and I. M. Reaney, "Niobate-based Microwave Dielectric Suitable for Third Generation Mobile Phone Base Station," *Appl. Phys. Lett.*, **79** [18] 2952-54 (2001).
2. K. Wakino, "Rescent Development of Dielectric Resonator Materials and Filters in Japan," *Ferroelectrics*, **91** 68-86 (1989).
3. W. Wersing, "High Frequency Ceramic Dielectrics and their Application for Microwave Components," pp. 67-119 in *Electronic Ceramics*. Edited by B. C. H. Steele. Elsevier Applied Science, London, U.K., 1991.
4. E. S. Kim, B. S. Chun, K. S. Bang, and J. C. Kim, "Microwave Dielectric Properties of $Ca_{1-x}Nd_{2x/3}TiO_3$ Ceramics," *J. Kor. Ceram. Soc.*, **38** [7] 672-77 (2001).
5. S. Nomura, "Ceramics for Microwave Dielectric Resonator," *Ferroelectrics*, **49** 61-70 (1983).
6. J. Y. Cho, K. H. Yoon, and E. S. Kim, "Strain Analysis for Quality Factor of the Layered $Mg_{0.93}Ca_{0.03}TiO_3$-$(Ca_{0.3}Li_{0.14}Sm_{0.42})$ TiO Ceramics," *J. Kor. Ceram. Soc.*, **39** [3] 222-25 (2002).
7. H. M. O'Bryan, J. Thomson, Jr., and J. K. Plourde, "A New BaO-TiO_2 Compound with Temperature Stable High Permittivity and Low Loss," *J. Am. Ceram. Soc.*, **57** 450-53 (1974).
8. E. S. Kim and H. G. Lee, "Effect of Bond Valence on Microwave Dielectric Properties of $(Pb_{1-x}Ca_x)(Ca_{1/3}Nb_{2/3})O_3$," *J. Kor. Ceram. Soc.*, **38** [7] 678-82 (2001).
9. B. W. Hakki and P. D. Coleman, "A Dielectric Resonator Method of Measuring Inductive Capacities in the Millimeter Range," *IRE Transaction Microwave Theory & Technology*, **8** 402-10 (1960).
10. M. U. Kohen, "Precision Lattice Constants from X-ray Powder Photographs," *Rev. Sci. Instrum.*, **6** 68-76 (1935).
11. R. D. Shannon, "Revised Effective Ionic Radii and Systematic Studies of Interatomic Distances in Halides and Chalcogenides," *Acta Crystallogr., Sect. A*, **32** [9] 751-67 (1976).
12. T. Hirata, "Oxygen Position, Octahedral Distortion, and Bond-valence Parameter from Bond Lengths in $Ti_{1-x}Sn_xO_2$ (0=x=1)," *J. Am. Ceram. Soc.*, **83** [12] 3205-07 (2000).
13. R. D. Shannon and G. R. Rossman, "Dielectric Constants of Silicate Garnets and the Oxide Additivity Rule," *Am. Mineral*, **77** 94-9 (1992).
14. J. N. Reimers, J. E. Greedan, C. V. Stager, and R. Kremer, "Crystal Structure and Magnetism in $CoSb_2O_6$ and $CoTa_2O_6$," *J. Solid State Chem.*, **83** 20-30 (1989).
15. H. J. Lee, H. M. Park, Y. K. Cho, Y. W. Song, S. Nahm, and J. D. Byun, "Microstructure Characterizations in Calcium Magnesium Niobate," *J. Am. Ceram. Soc.*, **84** [7] 1632-36 (2001).